Clays and Clay Minerals, Vol. 54, No. 6, 667–677, 2006.

HYDROTHERMAL SYNTHESIS OF Mg-RICH AND Mg-Ni-RICH KAOLINITE

MARIA BENTABOL[1], MARIA DOLORES RUIZ CRUZ[1,*], FRANCISCO JAVIER HUERTAS[2] AND JOSE LINARES[2]

[1] Departamento de Química Inorgánica, Cristalografía y Mineralogía, Facultad de Ciencias, Universidad de Málaga, Spain
[2] Estación Experimental del Zaidín, CSIC, Prof. Albareda 1, 18008 Granada, Spain

Abstract—Mg-rich kaolinite and Mg+Ni-rich kaolinite have been synthesized in hydrothermal experiments (200 and 400ºC) from poorly crystalline kaolinite and Mg- and Mg+Ni-bearing solutions. Al-rich serpentine and Al-rich chlorite were obtained as sub-products of the reactions. The formation of these phases occurred through a dissolution-precipitation mechanism that led to spherical kaolinite after short reaction times. A morphological evolution towards platy particles and stacks occurred at increasing run times.

Identification of the several phases was carried out using a combination of X-ray diffraction and transmission/analytical electron microscopy. Analytical data indicate that the Mg content in kaolinite increased as a function of the reaction time and temperature, reaching up to 0.46 atoms per half formula unit (a.p.h.f.u.). The measured (Mg+Ni) content reached up to 0.56 a.p.h.f.u.. Both the gradual increase of the *b*-cell parameter of kaolinite at increasing Mg contents and the presence of new bands on the FTIR spectra of the synthesized kaolinite point to a Mg-for-Al replacement in the octahedral sheet rather than to the presence of serpentine-like layers interstratified in the kaolinite structure.

Key Words—Al-rich Serpentine, FTIR, Hydrothermal Synthesis, Mg-rich Kaolinite, TEM/AEM, XRD.

INTRODUCTION

Minerals of the kaolin subgroup (kaolinite, dickite, nacrite and halloysite) are dioctahedral 1:1 phyllosilicates ($Al_2Si_2O_5(OH)_4$), which mainly originate from the alteration of Al-rich phases (e.g. feldspars, mica) either hydrothermally or by weathering. It is well known that their formation is favored in the presence of acid to neutral waters, with low cation concentrations (Millot, 1964).

It is rare for minerals of this group to contain appreciable amounts of elements other than Si and Al. Nevertheless, the presence of Fe^{3+} in natural kaolinites has been known for many years (*e.g.* Herbillon *et al*., 1976; Mestdagh *et al*., 1980; Cuttler, 1981; Stone and Torres Sánchez, 1988; Delineau *et al*., 1994; Gaite *et al*., 1997), Fe-bearing kaolinites originating mainly in Fe-rich environments such as tropical soils or associated with Fe ores. In addition, Cr-rich kaolinites have been described occasionally (*e.g.* Brookins, 1973; Maksimovic and Brindley, 1980; Maksimovic *et al*., 1981; Singh and Gilkes, 1991), in most cases associated with the hydrothermal alteration of ultrabasic rocks. Large degrees of ionic substitutions (Fe = 0.44 a.p.f.u.; Cr = 0.56 a.p.f.u. for $O_5(OH)_4$) have been described for halloysites (Newman and Brown, 1987). It appears, then, that the type of foreign cations present in the kaolinite structure depends mainly on the bulk-rock composition, whereas the amount of substitution appears to be controlled by the structure with the disordered varieties accepting larger amounts of substitutions (Brindley *et al*., 1986).

Natural kaolinites, however, do contain very small amounts of Mg (Deer *et al*., 1976; Newman and Brown, 1987). The largest Mg contents (~0.05 a.p.f.u.) have been described in Cr-halloysites formed during the alteration of ultrabasic rocks (Maksimovic *et al*., 1981).

Kaolinites with appreciable Fe contents have also been synthesized (*e.g.* Angel *et al*., 1975; Petit *et al*., 1990; Iriarte, 2003; Iriarte *et al*., 2005). Few data exist, however, indicating the presence of isomorphous substitutions of other cations (Cu, Ga, *etc*.) for ^{VI}Al in kaolinites (*e.g.* Angel *et al*., 1975; Meads *et al*., 1975; Petit *et al*., 1995; Martin *et al*., 1998), though there are no data on the synthesis of kaolinites containing appreciable amounts of Mg and Ni.

As the presence of foreign cations (*e.g.* Ti, Na, Ca) in the bulk kaolinite analyses can be due to the existence of submicroscopic impurities (mainly Ti oxides, smectite and mica), more sensitive techniques, such as transmission electron microscopy (TEM) and energy dispersive analyses are necessary in order to prove the absence of impurities. Nevertheless, the possibility that cations such as Fe, Mg or Ni in the kaolinite analyses (even in those obtained by analytical electron microscopy) can reflect the presence of mixed-layering of Mg-, Fe- or Ni-rich serpentine and kaolinite can be hardly be discounted by these techniques.

The present work is part of a more extensive study, designed to investigate the transformations of kaolinite from 200 to 400ºC, within a wide range of pH values and

* E-mail address of corresponding author:
mdruiz@uma.es
DOI: 10.1346/CCMN.2006.0540602

Table 1. Kaolinite particle size determined from low-magnification TEM images.

	Average particle size (Å)	*n*	σ
Ground kaolinite	489	295	180
Spherical particles (T-3h)	642	250	318
Spherical particles (T-1)	553	160	220
Spherical particles (TM-30)	769	280	315
Stack length (T-30)	2237	108	995
Stack thickness (T-30)	879	108	420
Platy particles (T-30)	1931	73	829

n: number of particles measured

at variable run times, in aqueous solutions containing variable amounts of Na, K, Li and Mg. Previous results (Bentabol *et al*., 2006) indicated that mica formation in K- and Na-bearing systems was accompanied by the formation of minor amounts of Mg-rich kaolinite. The purpose of this paper is to present the results obtained from a set of hydrothermal reactions carried out in K- and Na-free chemical systems, designed to favor Mg kaolinite formation. Two slightly different chemical systems (MgO-NiO-Al_2O_3-SiO_2-H_2O-HCl and MgO-Al_2O_3-SiO_2-H_2O) were used, and studied at temperatures of 200 and 400ºC.

METHODOLOGY

The starting material consisted of poorly crystalline kaolinite from Georgia (KGa-2, from The Clay Minerals Society Source Clays Repository, Purdue University, Indiana) used after intense grinding (HSM 100 vibration grinder). The HSM 100 vibration grinder consists of a cylindrical tungsten container (14 cm inner diameter) within which a tungsten ring (10 cm diameter) and a cylinder (8 cm diameter) are concentrically placed. Kaolinite was ground in amounts of 100 g for 120 min. After every minute of grinding the process was halted for 30 s to avoid overheating and after 5 min of grinding the process was halted for 90 s for the same purpose, following the method proposed by Drief and Nieto (1999). Transmission electron microscopy observations and granulometric analyses indicated that the ground kaolinite is composed of rounded particles with an average size of <0.1 μm (González Jesús *et al*., 2000) (Table 1). Grinding also led to amorphization of a large proportion of the kaolinite, as deduced from the presence of a broad diffraction band between 20 and 30º2θ (Figure 1). The impurities detected by X-ray diffraction (XRD) and transmission/analytical electron microscopy (TEM/AEM) consist of abundant grains of anatase and minor Fe oxide.

The reactions studied are summarized in Table 2. Reactions T and TM were performed at 200ºC and reaction TC at 400ºC. A solution:solid ratio = 1:15 was used in all the reactions. The hydrothermal treatments of reactions at 200ºC were conducted in 50 cm^3 Teflon-lined reactors (Parr 4744) (reaction T) and Ni reactors (Parr 4713) (reaction TM), which were maintained at a constant temperature of 200ºC (±3ºC), with reaction times from 5 to 30 days. Shorter times (3, 6 h and 1 day) were also used in some cases. Reactions at 400ºC were performed in a high-pressure Inconel 600 reactor (Parr 4740), with reaction times of 1, 3 and 6 h. At the end of the runs the reactors were quickly quenched in cold water. Reactions T and TM were planned initially for studying the possible influence of the pH on the Mg-for-Al replacement in kaolinite. Nevertheless, the use of Ni reactors in reaction TM, and the dissolution of Ni during the experiments, led to a more complicated chemical system than in reaction T.

The solid products of the reactions were characterized by XRD, Fourier transform infrared spectroscopy (FTIR) and TEM/AEM. The XRD patterns were obtained using a Siemens D-5000 powder diffractometer with CuKα radiation at 40 kV and 30 mA, with a step size of 0.02º2θ and a counting time of 1 s. X-ray diffraction patterns of randomly oriented samples were obtained between 2 and 65º2θ. Oriented samples were scanned between 2 and 30º2θ, in the air-dried state, after solvation with ethylene glycol (EG), and after heating at 350ºC.

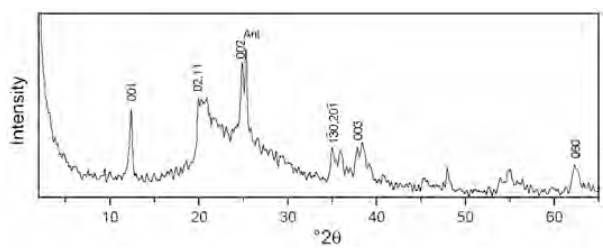

Figure 1. XRD pattern obtained from an unoriented sample of ground kaolinite. Ant: Anatase.

https://doi.org/10.1346/CCMN.2006.0540602 Published online by Cambridge University Press

Table 2. Reactions studied.

Reactions	Times	Temperature
1kln + 0.6 $Mg(OH)_2$	3 hours (T-3h), 1 day (T-1), 5 days (T-5) 15 days (T-15), 30 days (T-30)	200ºC
1kln + 0.6 $Mg(OH)_2$	1 hour (TC-1), 3 hours (TC-3), 6 hours (TC-6)	400ºC
1kln + 0.3 $Mg(OH)_2$+0.3 $MgCl_2$	5 days (TM-5), 15 days (TM-15), 30 days (TM-30)	200ºC

The FTIR spectra were recorded using KBr pellets (2 wt.% sample) in a Nicolet spectrometer (20XB), in the range 4000−400 cm^{-1}. The resolution was 2 cm^{-1} and 300 scans were accumulated to improve the signal to noise ratio in the spectra. To avoid grinding effects in the preparation of the discs, samples and KBr were gently mixed manually. The pellets were dried at 60ºC for 1 day before obtaining the spectra.

The TEM study was carried out using two instruments: (1) a Philips CM-20 microscope operated at 200 kV (CIC, University of Granada); and (2) a Jeol 3000 F, operated at 300 kV (University of Complutense), both fitted with an ultrathin window, solid-state Si(Li) detector for energy dispersive X-ray analysis (EDAX and OXFORD, respectively). The solid products were encased within an epoxy resin and then sliced. The atomic% was calculated by the Cliff-Lorimer thin-film ratio criteria (Lorimer and Cliff, 1976).

RESULTS

XRD results

A summary of the solid products identified by XRD is given in Table 3. Figure 2 shows the XRD patterns, obtained from unoriented samples, of the products of the reactions.

The XRD pattern of the solid products obtained from reaction T after very short reaction times (sample T-3h) shows kaolinite and brucite reflections. Both facts, the increase in intensity of the kaolinite reflections relative to the starting kaolinite (as compared with the anatase reflection), and the loss of the X-ray amorphous band present in the pattern of the starting kaolinite, indicate a process of dissolution-precipitation of kaolinite. The products formed from 1 day of reaction show similar XRD patterns, with intense kaolinite reflections. In addition, a well-defined reflection at 1.525 Å, clearly different from the more intense 06,33 reflection of kaolinite at ~1.49 Å) is also evident. The 1.525 Å peak was interpreted as the 060 reflection of a 7 Å di,trioctahedral phase. The presence of such a phase is, in part, confirmed by the presence of a reflection at 1.75 Å (008), intermediate in position between the 004 and $2\bar{2}2$ kaolinite reflections, and the presence of a reflection at 1.60 Å (207), both suggesting the presence of a lizardite-like di,trioctahedral structure (Bailey, 1984). Data from other experiments in the system Na_2O-K_2O-MgO-Al_2O_3-SiO_2-H_2O-HCl where only mica and serpentine formed, indicate that serpentine is similar to the 6(3) type synthesized by Gillery (1959). The cell parameters determined assuming a 6-layer orthogonal structure are: a = 5.28 Å; b = 9.17 Å; c = 42.42 Å.

Table 3. Solid products of the reactions as deduced from the XRD data.

Reaction	Solid phases
T-3h	Kaolinite + brucite
T-1	Kaolinite + 7 Å di,trioctahedral phase + (brucite)
T-5	Kaolinite + 7 Å di,trioctahedral phase + (brucite)
T-15	Kaolinite + 7 Å di,trioctahedral phase + quartz?
T-30	Kaolinite + 7 Å di,trioctahedral phase + quartz?
TM-5	Kaolinite
TM-15	Kaolinite
TM-30	Kaolinite
TC-1	Kaolinite + 7 Å di,trioctahedral phase + hydralsite
TC-3	Kaolinite + 7 Å di,trioctahedral phase + hydralsite
TC-6	Kaolinite + 7 Å di,trioctahedral phase + hydralsite

All the XRD patterns of the solid products of reaction TM are very similar, also showing the reflections of the recrystallized kaolinite, and the presence of a single 06,33 reflection at 1.49 Å. The presence of a badly defined reflection at ~4.16 Å suggests an improvement in the crystallinity of the recrystallized kaolinite relative to the products of reaction T.

The XRD patterns of the products of reaction TC show, in addition to the reflections of kaolinite and serpentine, a set of reflections (at 8.99, 3.42, 2.43 and 2.08 Å), ascribed to hydralsite (Roy and Osborn, 1954).

In all cases, the recrystallized kaolinite shows poorly defined 02,11 reflections, indicating abundant translation defects (Plançon and Zacharie, 1990).

TEM/AEM results

On the basis of the XRD results, five samples were selected for the TEM/AEM study: T-3h, T-1, T-30, TM-30 and TC-3. A summary of the solid products identified by TEM is given in Table 4.

The solid products of reaction T show a clear morphological and chemical evolution as a function of the reaction time. Images of the solid products of reaction T-3h taken at low magnification show spherical particles of kaolinite with sizes of the order of 600 Å

https://doi.org/10.1346/CCMN.2006.0540602 Published online by Cambridge University Press

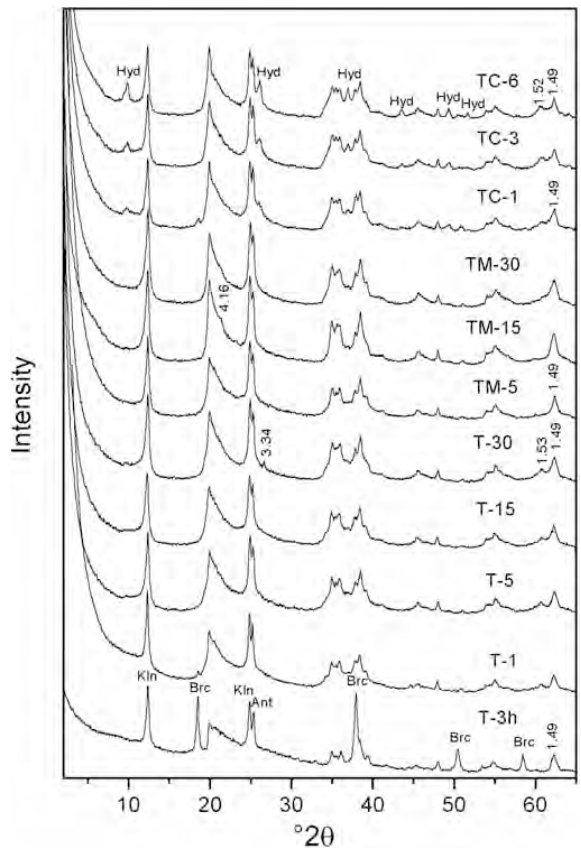

Figure 2. XRD patterns obtained from unoriented samples (range 2–65°2θ) of the solid products of the hydrothermal reactions. Kln: kaolinite; Brc: brucite; Ant: anatase; Hyd: hydralsite. Spacings in Å.

(Table 1) and stacks of brucite. Spherical particles of kaolinite occasionally include an anatase grain, as described by González Jesús *et al*. (2000). Spherical particles are rapidly damaged by the electron beam. Stacks of brucite show very variable sizes (Figure 3a). Although brucite shows intense and sharp peaks in the XRD patterns, obtaining diffraction images is difficult because the brucite particles are also rapidly damaged.

Low-magnification images of the solid products of reaction T-1 show two main types of kaolinite morphologies: spherical particles (with sizes between 200 and 1000 Å in diameter) and larger platy particles (up to 1 μm long) (Figure 3b). Large particles of kaolinite are notably more resistant to the electron beam than the spherical ones. The SAED patterns obtained from the platy particles show 00*l* reflections with 7 Å periodicity and almost continuous 0*kl* reflection rows, indicating important structural disorder (Figure 3b, inset). The rapid damage of kaolinite from this sample prevented us from obtaining lattice-fringe images. Another consequence of the damage is the loss of Al, most of the analyses obtained showing an excess of Si. Thus, the calculated formulae display small octahedral occupancy (Table 5). It is also possible that the excess Si suggests

Table 4. Solid products of the reactions as deduced from the TEM/AEM data.

Reaction	Solid phases
T-3h	Kaolinite + brucite
T-1	Mg kaolinite + (brucite) + silica + (Mg serpentine)
T-30	Mg-kaolinite + Al-rich serpentine + silica
TM-30	Mg-Ni-rich kaolinite + Al-rich serpentine + silica
TC-3	Mg-rich kaolinite + Al-rich serpentine + Al-rich chlorite

https://doi.org/10.1346/CCMN.2006.0540602 Published online by Cambridge University Press

Table 5. Representative AEM data for kaolinites (calculated for $O_5(OH)_4$)

	T-15	T-30		TM-30		TC-3	
Si	2.17	2.00	2.01	1.95	1.64	1.98	2.01
^{IV}Al	0.00	0.00	0.00	0.05	0.36	0.02	0.00
^{VI}Al	1.70	1.86	1.66	1.81	1.74	1.89	1.67
Fe	0.02	0.05	0.08	0.07	0.03	0.00	0.04
Mg	0.08	0.13	0.35	0.14	0.30	0.17	0.42
Ni	0.00	0.00	0.00	0.06	0.23	0.00	0.00
Σoct.	1.80	2.04	2.09	2.08	2.30	2.06	2.13

that the kaolinite particles are covered with a thin coating of X-ray amorphous silica, as observed by Jepson and Rowse (1975). In spite of the fact that Mg is present in all of the analyses, the Mg content is small ($\leqslant$0.08 a.p.f.u.), calculated for $O_5(OH)_4$). Most analyses from this and the other samples show small amounts of Fe, probably coming from dissolution of Fe oxide present in kaolinite as impurities.

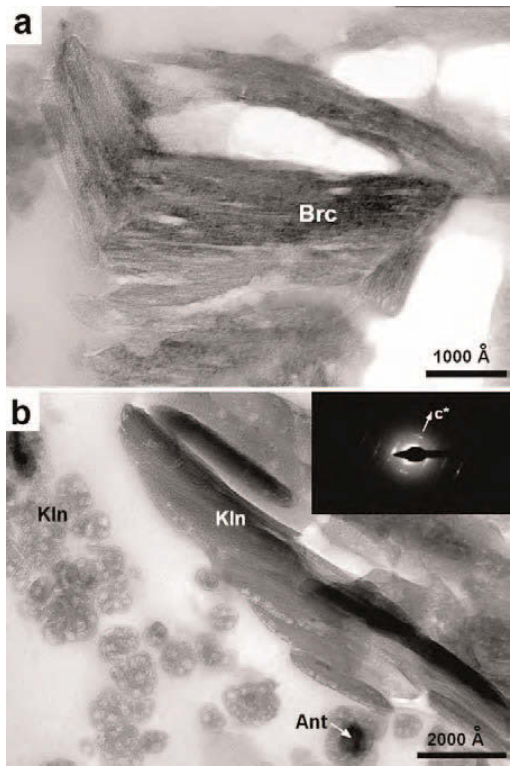

Figure 3. (a) Low-magnification TEM image of the solid products of reaction T-3h, showing a brucite (Brc) stack. (b) Low-magnification TEM image of the solid products of reaction T-1 showing the different morphologies of kaolinite. Inset: *b**-*c** SAED pattern of the largest kaolinite particle, showing the 7 Å periodicity and the presence of almost continuous 0*kl* reflection rows. Ant: anatase; Kln: kaolinite.

Increasing reaction times (sample T-30) causes the disappearance of spherical kaolinite. Low-magnification TEM images of this sample shows the prevalence of large platy particles of kaolinite (of the order of 2000 Å, Table 1) and aggregates of fine-grained particles of a Mg-rich phase (Figure 4a). The lattice-fringe images of kaolinite show the typical 7 Å periodicity and regularity of the kaolinite layers (Figure 4b). The AEM data of kaolinite indicate that all particles contain Mg (and minor Fe), in greater amounts than kaolinite from sample T-1. The Mg+Fe content ranges from 0.11 to 0.43.

Most analyses of Mg-rich phases show a notable excess of Si, indicating that these phases are either mixed or coated by silica. Only two of the analyses obtained appear to be silica-free (Table 6). Both show high Mg contents, suggesting a chlorite or serpentine-like composition. Although lattice-fringe images of these aggregates could not be obtained, the formulae were calculated for an $O_5(OH)_4$ anionic basis, as the XRD patterns of this sample show only reflections corresponding to 7 Å phyllosilicates. The formulae range obtained from an almost trioctahedral serpentine (^{VI}Al = 0.20 a.p.f.u. and total octahedral occupancy

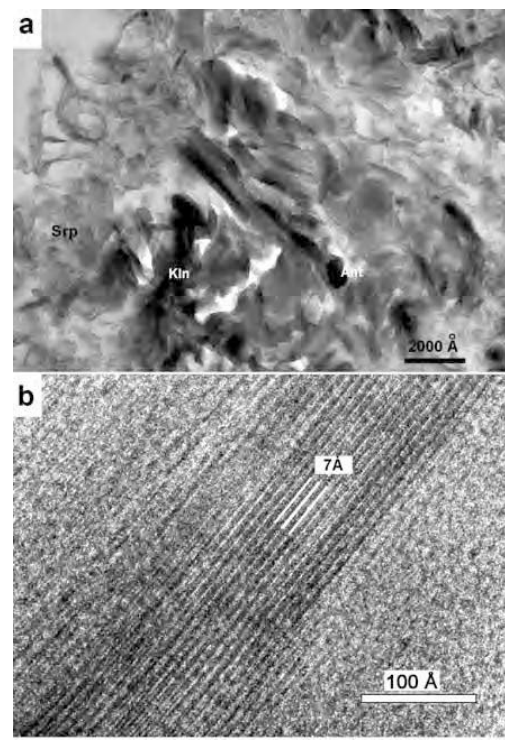

Figure 4. (a) Low-magnification TEM image of the solid products of reaction T-30. Kln: kaolinite; Ant: anatase; Srp: serpentine. (b) Lattice-fringe image of kaolinite from sample T-30, showing the regular 7 Å periodicity.

https://doi.org/10.1346/CCMN.2006.0540602 Published online by Cambridge University Press

Table 6. Representative AEM data for serpentine (calculated for $O_5(OH)_4$) and chlorite (calculated for $O_{10}(OH)_8$)

	T-30		TM-30		TC-3	
	(Srp)	(Srp)	(Srp)	(Srp)	(Srp)	(Chl)
Si	2.00	1.89	1.79	1.83	1.82	3.40
^{IV}Al	0.00	0.11	0.21	0.17	0.18	0.60
^{VI}Al	0.20	0.80	1.11	1.15	1.16	2.04
Fe	0.10	0.02	0.05	0.03	0.02	0.08
Mg	2.55	1.83	1.16	0.79	1.32	3.12
Ni	0.00	0.00	0.20	0.52	0.00	0.00
Σoct.	2.85	2.65	2.52	2.49	2.50	5.24
T. oct.	2.90	2.66	2.55	2.51	2.51	5.28

T. oct.:
theoretical values assuming Σoct.= $3-1/2(^{VI}Al-^{IV}Al)$

(Σoct.) = 2.84 a.p.f.u.) to a di,trioctahedral composition (^{VI}Al = 0.80 a.p.f.u. and Σoct. = 2.66 a.p.f.u.) (Table 6). In addition, all serpentine analyses show small but uniform Cl contents (not quantified).

The solid products of reaction TM-30 show a variety of morphologies, as observed by TEM (Figure 5): small particles of spherical kaolinite, similar to those found in reactions T, stacks of kaolinite, large particles of platy kaolinite, and minor amounts of aggregates of fine-grained particles of a Mg-Ni-rich phase and aggregates of fine particles of silica. The presence of Ni in the solid phases of this reaction is due to the dissolution of the Ni reactors. For different reactions T, the different kaolinites formed were all stable against the electron beam. The lattice-fringe images of kaolinite are similar to those found for sample T-30. Kaolinites show a range of chemical compositions in both the tetrahedral and the octahedral sheets. The more Al-rich kaolinites show Mg+Ni+Fe contents = 0.16 a.p.f.u., scarce tetrahedral substitution of Al for Si, and octahedral occupancy of

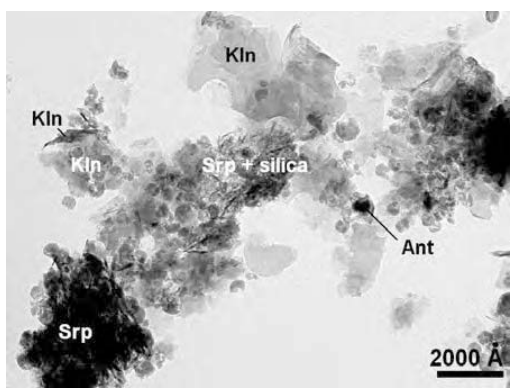

Figure 5. Low-magnification TEM image showing the sizes and morphologies of the phases identified in the products of reaction TM-30: spherical and platy particles and small packets of kaolinite (Kln) and aggregates of serpentine (Srp) and silica. Anatase (Ant) grains are also visible in this image.

~2 a.p.f.u. (Table 5). The Mg+Ni+Fe content, however, reaches up to 0.56 a.p.f.u. in some of the particles analyzed, which show, in addition, greater tetrahedral substitution, and octahedral occupancy in the order of 2.3 a.p.f.u. Generally (but not always), the spherical particles show the greatest Al contents whereas the largest Mg+Ni contents were determined in stacks and platy particles. The Mg/(Mg+Ni+Fe) ratio is variable from particle to particle, ranging from 0.5 to 0.7.

The formulae of the Mg-Ni-rich phases have also been calculated for $O_5(OH)_4$ (Table 6). The formulae obtained correspond to an Al-rich serpentine with scarce tetrahedral substitution and high Mg+Ni-for-Al octahedral substitution. These formulae clearly deviate from those of the typical Al-rich serpentines (amesite and Al-lizardite) since the ^{VI}Al is notably greater than the ^{IV}Al, in such a way that the octahedral occupancy (~2.5 a.p.f.u.) is typical of a di,trioctahedral phase. The Ni content in the serpentine is also variable from particle to particle, the Mg/(Mg+Ni) ratio ranging from 0.60 to 0.85.

The TEM/AEM data of the solid products of reaction TC-3 reveal the presence of large crystals of kaolinite, some of which are up to 2 μm long, and smaller packets of a Mg-rich phase (Figure 6a). The lattice-fringe images of kaolinite show a dominant 7 Å periodicity and, locally, structural defects such as layer terminations (Figure 6b). The AEM data for kaolinite (Table 5) indicate that the Si content is near 2.0 a.p.f.u. in all the analyses obtained, whereas the Mg+Fe content in the octahedral sheet varies between 0.17 and 0.46 a.p.f.u. The octahedral occupancy ranges between 2.06 and 2.13 a.p.f.u.

Most lattice-fringe images of the Mg-rich particles show a dominant 7 Å periodicity, characteristic of serpentine minerals. Structural defects, such as bending of layers and layer terminations are frequent. In addition, these images show the presence of occasional 14 Å (chlorite-like?) layers, interstratified in the serpentine structure (Figure 7a). These serpentine particles show chemistries similar to those determined in sample TM-30 (Table 6) although the particle size is greater in sample TC-3. The octahedral occupancy is of the order of 2.5 a.p.f.u., corresponding to a di,trioctahedral structure.

Some other packets with Mg-rich composition however, display lattice-fringe images with a main 14 Å periodicity (Figure 7b), as also shown by the Fourier transforms. The structural formulae have been calculated for $O_{10}(OH)_8$, assuming a chlorite-type structure (Table 6). The formulae reveal high Si contents, high ^{VI}Al contents and low octahedral occupancy (~5.24 a.p.f.u.), which is near that of a di- or a di,trioctahedral phase.

Infrared spectroscopy results

The FTIR spectra of some selected samples are shown in Figure 8. The four high-frequency bands of typical kaolinite (at 3696, 3670, 3650,and 3620 cm^{-1}) are present in the spectrum of the source clay KGa-2

https://doi.org/10.1346/CCMN.2006.0540602 Published online by Cambridge University Press

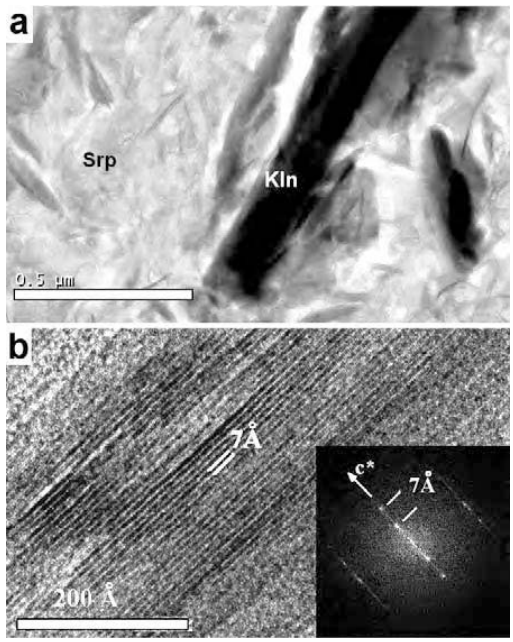

Figure 6. (a) Low-magnification image of kaolinite (Kln) and serpentine (Srp) formed through reaction TC-3. (b) Lattice-fringe image of kaolinite from sample TC-3. Layer terminations are observed in the upper left side of the packet. The inset Fourier transform pattern shows a 7 Å periodicity.

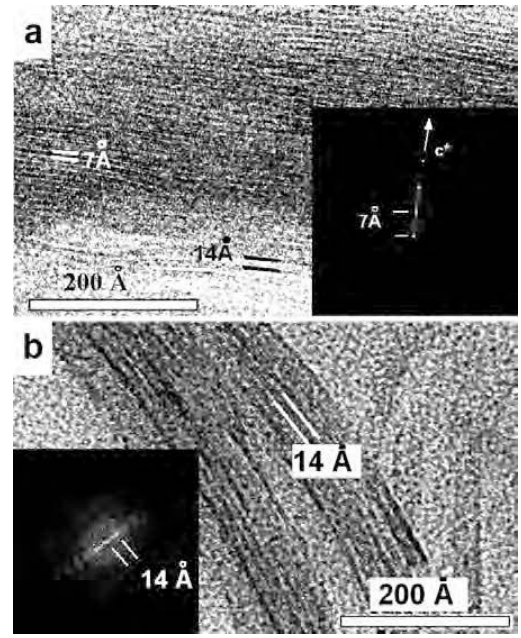

Figure 7. Lattice-fringe images of Mg-rich phases of sample TC-3. (a) This serpentine packet shows dominant 7 Å periodicity. Bending and layer terminations as well as 14 Å fringes are frequent in this packet. The inset Fourier transform also shows the 7 Å periodicity. (b) This curved packet shows a dominant 14 Å (chlorite-like) periodicity, as also shown by the Fourier transform.

(Figure 8a). The complete assignment of these bands is still in dispute although it is generally accepted that the band near 3620 cm^{-1} arises from the internal OH groups whereas that near 3700 cm^{-1} corresponds to the inner-surface OH groups (Russell and Fraser, 1994). The low intensity of the 3668 cm^{-1} band reflects abundant disorder, which could arise, in part, from the presence of small amounts of dickite- or nacrite-like stacking in the kaolinite structure (Farmer, 1974).

All spectra in Figure 8 have been normalized to a common intensity of the principal Si–O stretching band to favor the comparison. Grinding-induced disorder is reflected in the spectrum of the ground kaolinite as there is a notable decrease in the intensity of the four OH-stretching bands and the increase of the 3621 cm^{-1} band relative to the higher-frequency band (Figure 8a). At increasing isomorphic substitution, the relative increase of the lowest-frequency OH-stretching band is enhanced in such a way that the spectrum of sample TC-6 strongly resembles that of dickite. In addition, the maximum of the bands at 3696 and 3668 cm^{-1} shifted to slightly higher frequencies, probably reflecting the contribution of the Mg-OH-Al vibrations.

The low-frequency zone of the spectra of the hydrothermally treated kaolinites (Figure 8b) reveals a notable decrease of the relative intensity of the δAl_2OH bands, as compared with the spectra of the KGa-2 kaolinite. The spectrum of sample TC-6 shows, in addition, a very small band at 612 cm^{-1}, which can be ascribed to the OH-deformation band of serpentine (Russell and Fraser, 1994). Moreover, this spectrum shows a weak band at lower frequency than the δAl-OH bands (844 cm^{-1}), which probably corresponds to the deformation of the Al-OH-Mg groups.

Study of the solutions

The evolution of the pH and the Si, Al and Mg concentrations in the solutions, at increasing reaction times, is shown in Table 7. As observed, the high initial pH of the solutions (8–9) decreases to the range 6.0–6.7 as the reactions progress. A first, lowering of the pH is observed after a short reaction time, as a consequence of the dissolution of the kaolinite. This is followed by a slight increase and a later stabilization. Similarly, the early increase of the Si and Al contents and their later decrease also reflect the dissolution-precipitation stages.

DISCUSSION

As Mg-rich kaolinites had not been described previously, some aspects of their structure, chemistry and genesis will be discussed below.

https://doi.org/10.1346/CCMN.2006.0540602 Published online by Cambridge University Press

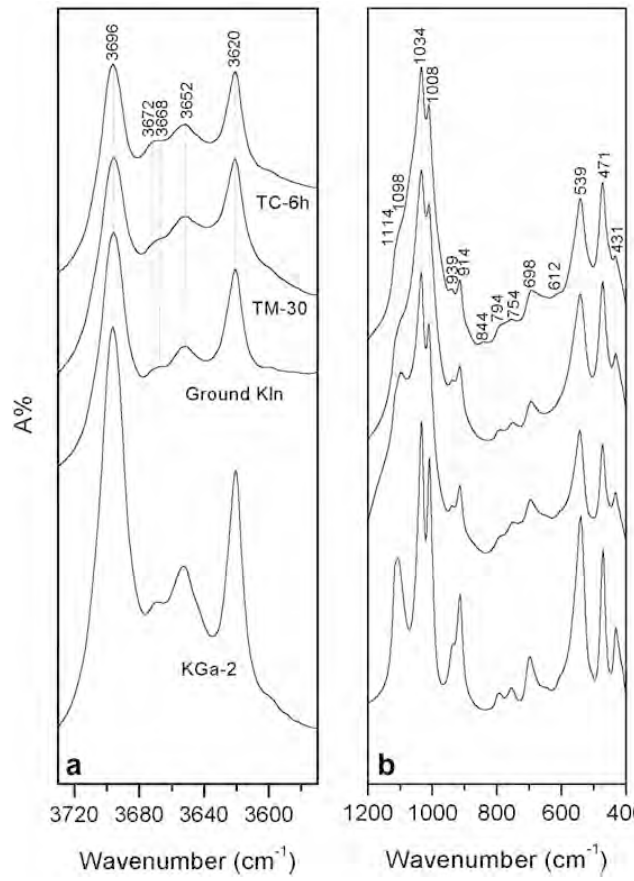

Figure 8. FTIR spectra of the starting materials and selected products of the hydrothermal reactions: (a) OH-stretching zone; (b) low-frequency zone.

Mg-rich and Mg-Ni-rich kaolinites vs. kaolinite-serpentine interstratifications

Although the presence of Mg- or Ni-bearing impurities in the recrystallized kaolinite can be ruled out from the TEM/AEM study, the possibility that Mg- or Ni-rich particles represent interstratifications of Mg- or Ni-serpentine and kaolinite cannot be discounted on the basis of these data. Nevertheless, some other criteria, such as the evolution of the *b* cell parameter and the presence of specific bands on the FTIR spectra have been used previously to prove the presence of Fe in the octahedral sheet of Fe-rich kaolinites (*e.g.* Petit *et al*., 1990; Iriarte *et al*., 2005).

In our case, differences in ionic radius between Al^{3+}, Mg^{2+} and Ni^{2+} suggest that the linear correlation between the cell parameters (mainly the *b* parameter) and the degree of isomorphous substitution must also exist. The exact determination of the spacing of the 06,33 reflection of kaolinites in the several reactions was carried out using the 101 reflection of anatase as an internal standard. Figure 9 shows a plot of the *b* cell parameters, deduced from the position of the 06,33 reflection of kaolinite against the main $\%^{VI}Al$, deduced from the AEM analyses. As expected, the *b* cell

Table 7. pH, Si, Al and Mg contents (mmol/L) in the solutions.

Reaction	pH	Si	Al	Mg
T-0	8.94	0.00	0.00	158.53
T-5	6.59	27.62	8.34	25.78
T-15	5.79	29.07	7.51	16.19
T-30	6.70	20.58	4.34	12.19
TM-0	8.09	0.00	0.00	158.60
TM-5	5.68	31.48	8.04	124.80
TM-15	7.06	25.46	4.19	129.86
TM-30	6.00	13.24	0.76	135.21
TC-0	7.98	0.00	0.00	158.63
TC-1h	4.49	22.75	7.81	39.27
TC-3h	6.05	24.74	4.91	38.06

https://doi.org/10.1346/CCMN.2006.0540602 Published online by Cambridge University Press

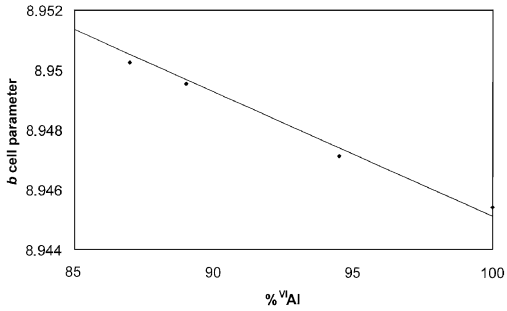

Figure 9. Plot of the calculated *b* cell parameter of the Mg-kaolinites *vs*. the mean ^{VI}Al content (%) as deduced from AEM data.

parameter of kaolinite increases parallel to the Mg- (or Mg+Ni) content (from 8.945 to 8.953 Å). Nevertheless, this increase is notably smaller than that observed in Fe-substituted kaolinites (*e.g.* Petit and Decarreau, 1990; Iriarte *et al*., 2005), suggesting that the position of the 06,33 reflection is also influenced by the position of the 331 reflection.

On the other hand, the FTIR spectra also point to the presence of discrete particles of Mg- and Mg-Ni-rich kaolinites. The main modifications observed in the spectra of the hydrothermally treated kaolinite were: (1) the relative decrease in intensity of the υAl_2OH and δAl_2OH bands with the increase in Mg content; (2) the shift of the 3668 cm^{-1} band towards higher frequencies; and (3) the presence of a new band at 844 cm^{-1}. The decrease in intensity of the Al_2OH bands has been observed previously in synthetic Fe kaolinites and Cu kaolinites (Petit and Decarreau, 1990; Petit *et al*., 1995) and interpreted as proof of the octahedral replacement. On the other hand, the modifications observed in the FTIR spectra also suggest that Mg (or Mg and Ni) occupy the octahedral positions in the synthetic kaolinite.

A plot of the Al *vs*. (Mg±Ni±Fe) compositional fields of the several phases identified by TEM/AEM is given in Figure 10. This plot reveals some significant features: (1) although the number of serpentine analyses is small (due to the frequent presence of silica coating the serpentine particles), it is evident that the composition of the Mg phases associated with kaolinite in the several samples ranges from pure Mg phases (brucite) in the sample with the lowest Mg substitution (T-3h) to Al-rich phases (in samples TM-30 and TC-3), indicating that increasing reaction times or increasing temperature favor the isomorphic substitutions in both kaolinite and serpentine. On the other hand, a continuous range of Mg- (or Mg+Ni)-for-Al substitution is observed in all samples except in TC-3 (probably due to the smaller number of analyses available). Thus, although the presence of some serpentine-like layers interstratified in the kaolinite structure cannot be completely ruled out, all these facts suggest that Mg and Ni are replacing Al in the octahedral sheet of the kaolinite structure.

Mechanisms of isomorphic substitution in kaolinite and serpentine

As indicated above, the most commonly described substituted kaolinites contain Fe^{3+}. The substitution of Fe^{3+} for Al^{3+} does not lead to changes in the octahedral charge, and the Fe-rich kaolinites are dioctahedral, at the same time as the tetrahedral positions are completely filled by Si (Petit and Decarreau, 1990; Iriarte *et al*., 2005). Petit *et al*. (1995) synthesized kaolinites containing Cu^{2+} but they did not present the formulae of the Cu-substituted kaolinites.

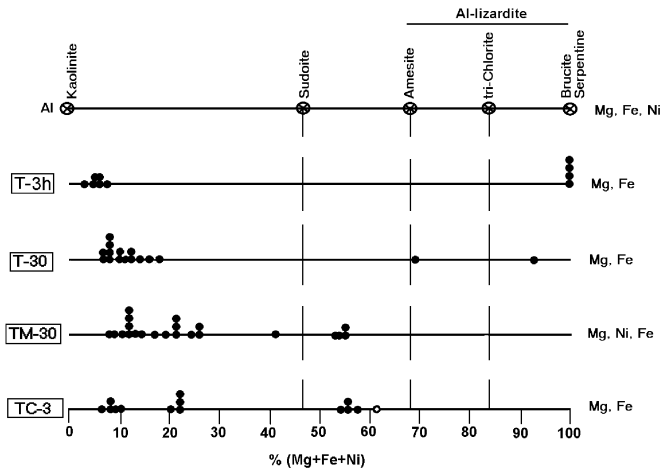

Figure 10. Plot of the compositional fields of the phases characterized by AEM in several samples, on an Al-(Mg,Ni,Fe) linear diagram. The positions of other mineral phases are marked in the upper line.

https://doi.org/10.1346/CCMN.2006.0540602 Published online by Cambridge University Press

Two mechanisms are possible for the isomorphous replacement when the new cations are divalent, as is the case for Mg and Ni: (1) the octahedral substitution of Mg^{2+} for Al^{3+} is coupled with a parallel Al^{3+}-for-Si^{4+} substitution in the tetrahedral sheet. In this case, the octahedral occupancy is near 2 a.p.f.u., and the substituted phase remains dioctahedral. This type of replacement (Tschermak-type substitution) is common in all of the phyllosilicates. (2) The octahedral substitution of Mg^{2+} for Al^{3+} is not coupled with a parallel tetrahedral substitution, and the octahedral occupancy increases in proportion to the degree of octahedral replacement. In our case, this replacement could follow the scheme: $2Al^{3+} + 1\square = 3\ Mg^{2+}$. This type of replacement is common in some di,trioctahedral chlorites where the ^{VI}Al content is clearly greater than the ^{IV}Al content and the octahedral occupancy is 5 a.p.f.u. In most kaolinites formed in our experiments (samples T-15, T-30 and TC-3), the tetrahedral Si content is near 2.0 a.p.f.u., and as a consequence, the total octahedral occupancy is >2 a.p.f.u. In sample TM-30, however, the tetrahedral substitutions are important but not sufficient to compensate for the large octahedral replacement, and the octahedral occupancy is clearly >2.0 a.p.f.u. The factors that control the prevalence of one or other type of replacement are not clear, but the presence of Ni in the octahedral sheet appears to favor the Tschermak-type substitution.

In the case of the serpentines, the ^{VI}Al content (~1.1 a.p.f.u.) is clearly greater than the ^{IV}Al content (~0.2 a.p.f.u.) and the substitution mechanisms, similar to those described in some Al-rich chlorites (Foster, 1962; Bailey, 1984), lead to di,trioctahedral phases. The octahedral occupancy is determined by the difference between ^{VI}Al and ^{IV}Al contents, with $\Sigma oct. = 3-1/2(^{VI}Al-^{IV}Al)$.

Stability vs. metastability of Mg-rich and Mg-Ni-rich kaolinites and Al-rich serpentines

As Mg- and Mg-Ni-rich kaolinites have not been described previously, it is difficult to evaluate the stability of these phases in natural environments. Previous data about the Mg content in Cr-bearing kaolinites suggest, however, that these types of kaolinites must be rare, and could be found in Mg-rich environments, *e.g.* where ultrabasic rocks are being altered.

On the other hand, Al-rich serpentines (amesite and Al-rich lizardite) are also rare minerals mainly formed in high-Al environments (Bailey, 1991; Wicks and O'Hanley, 1991). Thus, the presence of high concentrations of both Al and Mg (or Al, Mg and Ni) in solution appears to be a necessary condition for the formation of the assemblage Mg-rich kaolinite (or Mg-Ni-rich kaolinite) + Al-rich serpentine. Indeed, it is known that the Al and Ni contents in serpentines are largely controlled by the bulk composition of the rocks in which they occur and not by the crystal chemical restrictions of the crystal structure (Wicks and O'Hanley, 1991).

The fact that the compositions of both kaolinite and serpentine do not change appreciably at increasing temperature suggests that the Mg-rich kaolinite + Al-rich serpentine assemblage is stable at 200ºC. At 400ºC, on the contrary, kaolinite gives rise to hydralsite and the Al-rich serpentine is accompanied by a di,trioctahedral chlorite of similar composition, suggesting that Al-rich serpentine is not stable at 400ºC and evolves to chlorite. These later observation are in accordance with the data of Gillery (1959), who described the synthesis of an Al-rich lizardite as being similar to that obtained in our experiments; below 500ºC, but above 500ºC a chlorite of similar composition was the stable phase.

CONCLUSIONS

The hydrothermal reaction of kaolinite (at 200ºC and 400ºC) in the presence of Mg- or Mg+Ni-bearing solutions yielded the assemblage Mg±Ni-rich kaolinite + Al-rich serpentine. Both the gradual increase of the *b* cell parameter of kaolinite at increasing isomorphic substitution and the presence of a new band in the OH-deformation region of the spectra suggest that the divalent cations Mg^{2+} and Ni^{2+} substitute for Al^{3+} in the octahedral sheet of the kaolinite. The high level of substitution (up to 0.56 a.p.f.u.) is probably favored by the abundant structural disorder of the recrystallized kaolinite.

The assemblage Mg-rich kaolinite + Al-rich serpentine appears to be stable at 200ºC, whereas at 400ºC, kaolinite gives rise to hydralsite, and serpentine appears to evolve towards an almost dioctahedral chlorite. This assemblage, which has not been described in natural environments, would probably require unusual Al- and Mg-rich chemical systems.

ACKNOWLEDGMENTS

The authors are grateful to D.D. Eberl and R.J. Pruett, whose suggestions and corrections notably improved the manuscript, and to J.L. Baldonedo, A. Gómez and M.M. Abad for help with obtaining the TEM/AEM data. This study received financial support from Project BTE-2003-01382 (Ministerio de Educación y Cultura, Spain) and from the Research Group RNM-199.

REFERENCES

Angel, B.R., Richards, K. and Jones, J.P.E. (1975) The synthesis, morphology, and general properties of kaolinites specifically doped with metallic ions, and defects generated by irradiation. Pp. 297–304 in: *Proceedings of the International Clay Conference*, 1975.

Bailey, S.W. (1984) Structures of layer silicates. Pp. 1–123 in: *Crystal Structures of Clay Minerals and their X-ray Identification* (G.W. Brindley and G. Brown, editors). Monograph **5**, Mineralogical Society, London.

Bailey, S.W. (1991) Structures and composition of other trioctahedral 1:1 phyllosilicates. Pp. 169–188 in: *Hydrous*

Phyllosilicates (exclusive of micas) (S.W. Bailey, editor). Reviews in Mineralogy, **19**. Mineralogical Society of America, Washington, D.C.

Bentabol, M., Ruiz Cruz, M.D., Huertas, F.J. and Linares, J. (2006) Chemical and structural variability of illitic phases formed from kaolinite in hydrothermal conditions. *Applied Clay Science*, **32**, 111–124.

Brindley, G.W., Chih-Chun, K., Harrison, J.L., Lipsicas, M. and Raythatha, R. (1986) Relation between structural disorder and other characteristics of kaolinites and dickites. *Clays and Clay Minerals*, **34**, 239–249.

Brookins, D.G. (1973) Chemical and X-ray investigation of chromiferous kaolinite ('miloschite') from the Geysers, Sonoma County, California. *Clays and Clay Minerals*, **21**, 421–422.

Cuttler, A.H. (1981) Further studies of ferrous iron doped synthetic kaolinite dosimetry of X-ray induced effects. *Clay Minerals*, **16**, 69–80.

Deer, W.A., Howie, R.A. and Zussman, M.A. (1976) *Rock Forming Minerals vol. 3 - Sheet Silicates*. Longman, Essex, UK, 270 pp.

Delineau, T., Allard, T., Muller, J.P., Barrès, O., Yvon, J. and Cases, J.M. (1994) FTIR reflectance vs. EPR studies of structural iron in kaolinites. *Clays and Clay Minerals*, **42**, 308–320.

Drief, A. and Nieto, F. (1999) The effect of dry grinding on the Mulhacén antigorite. *Clays and Clay Minerals*, **47**, 417–424.

Farmer, V.C. (1974) The layer silicates. Pp. 331–365 in: *The Infrared Spectra of Minerals* (V.C. Farmer, editor). Monograph **4**, Mineralogical Society, London.

Foster, M.D. (1962) Interpretation of the composition and a classification of the chlorites. *US Geological Survey Professional Paper*, **414–A**, 1–33.

Gaite, J.M., Ermakoff, P. and Muller, J.P. (1997) Characterization and origin of two Fe^{3+} EPR spectra in kaolinite. *Physics and Chemistry of Minerals*, **20**, 242–247.

Gillery, F.H. (1959) The X-ray study of synthetic Mg-Al serpentines and chlorites. *American Mineralogist*, **44**, 143–152.

González Jesús, J., Huertas, F.J., Linares, J. and Ruiz Cruz, M.D. (2000) Textural and structural transformations of kaolinites in aqueous solutions. *Applied Clay Science*, **17**, 245–263.

Herbillon, A.J., Mestdagh, M.M., Vielvoye, L. and Derouane, E.G. (1976) Iron in kaolinites with special reference to kaolinite from tropical soils. *Clay Minerals*, **11**, 201–220.

Iriarte, I. (2003) Formación de minerals de la arcilla en el sistema SiO_2-Al_2O_3-Fe_2O_3-MgO-Na_2O-H_2O entre 150 y 225ºC. PhD thesis, University of Granada, Spain.

Iriarte, I., Petit, S., Huertas, F.J., Fiore, S., Grauby, O., Decarreau, A. and Linares, J. (2005) Synthesis of kaolinite with a high level of Fe^{3+} for Al substitution. *Clays and Clay Minerals*, **53**, 1–10.

Jepson, W.B. and Rowse, J.B. (1975) The composition of kaolinite – an electron microscope microprobe study. *Clays and Clay Minerals*, **23**, 310–317.

Lorimer, G.W. and Cliff, G. (1976) Analytical electron microscopy of minerals. Pp. 506–519 in: *Electron Microscopy in Mineralogy* (H.R. Wenk, editor). Springer-Verlag, New York.

Maksimovic, Z. and Brindley, G.W. (1980) Hydrothermal alteration of a serpentine near Takovo, Yugoslavia, to Cr-bearing illite/smectite, kaolinite, tosudite and halloysite. *Clays and Clay Minerals*, **28**, 295–302.

Maksimovic, Z., White, J.L. and Logar, M. (1981) Chromium bearing kaolinite from Teslic, Yugoslavia. *Clays and Clay Minerals*, **29**, 213–218.

Martin, F., Petit, S., Decarreau, A., Ildefonse, Ph., Grauby, O., Beziat, D., Parseval, P. and Noack, Y. (1998) Ga/Al substitution in synthetic kaolinites and smectites. *Clay Minerals*, **33**, 231–241.

Meads, R.E. and Malden, P.S. (1975) Electron-spin resonance in natural kaolinites containing Fe^{3+} and other transition metal ions. *Clay Minerals*, **10**, 313–345.

Mestdagh, M.M., Vielvoye, L. and Herbillon, A.J. (1980) Iron in kaolinite. II. The relationship between kaolinite crystallinity and iron content. *Clay Minerals*, **15**, 1–13.

Millot, G. (1964) *Géologie des Argiles*. Masson, Paris, 499 pp.

Newman, A.C.D. and Brown, G. (1987) The chemical constitution of clays. Pp. 1–128 in: *Chemistry of Clays and Clay Minerals*. Monograph **6**, Mineralogical Society, London.

Petit, S. and Decarreau, A. (1990) Hydrothermal (200ºC) synthesis and crystal chemistry of iron-rich kaolinites. *Clay Minerals*, **25**, 181–196.

Petit, S., Decarreau, A., Mosser, C., Ehret, G. and Grauby, O. (1995) Hydrothermal synthesis (250ºC) of copper-substituted kaolinites. *Clays and Clay Minerals*, **43**, 482–494.

Plançon, A. and Zacharie, C. (1990) An expert system for the structural characterization of kaolinites. *Clay Minerals*, **25**, 249–260.

Roy, R. and Osborn, E.F. (1954) The system Al_2O_3-SiO_2-H_2O. *American Mineralogist*, **39**, 853–885.

Russell, J.D. and Fraser, A.R. (1994) Infrared methods. Pp. 11–67 in: *Clay Mineralogy: Spectroscopic and Chemical Determinative Methods* (M.J. Wilson, editor). Chapman & Hall, London.

Singh, B. and Gilkes, R.J. (1991) Weathering of a chromian muscovite to kaolinite. *Clays and Clay Minerals*, **39**, 571–579.

Stone, W.E.E. and Torres Sánchez, R.M. (1988) Nuclear magnetic resonance spectroscopy applied to minerals. Part 6. Structural iron in kaolinite as viewed by proton magnetic resonance. *Journal of the Chemical Society, Faraday Transactions*, **84**, 117–132.

Wicks, F.J. and O'Hanley, D.S. (1991) Serpentine minerals: structures and petrology. Pp. 91–167 in: *Hydrous Phyllosilicates (exclusive of micas)* (S.W. Bailey, editor). Reviews in Mineralogy, **19**. Mineralogical Society of America, Washington, D.C.

(*Received 8 February 2006; revised 22 May 2006; Ms. 1139; A.E. Peter J. Heaney*)